Volume 14
Number 34
14 September 2022
Pages 12185-12500

Nanoscale

rsc.li/nanoscale

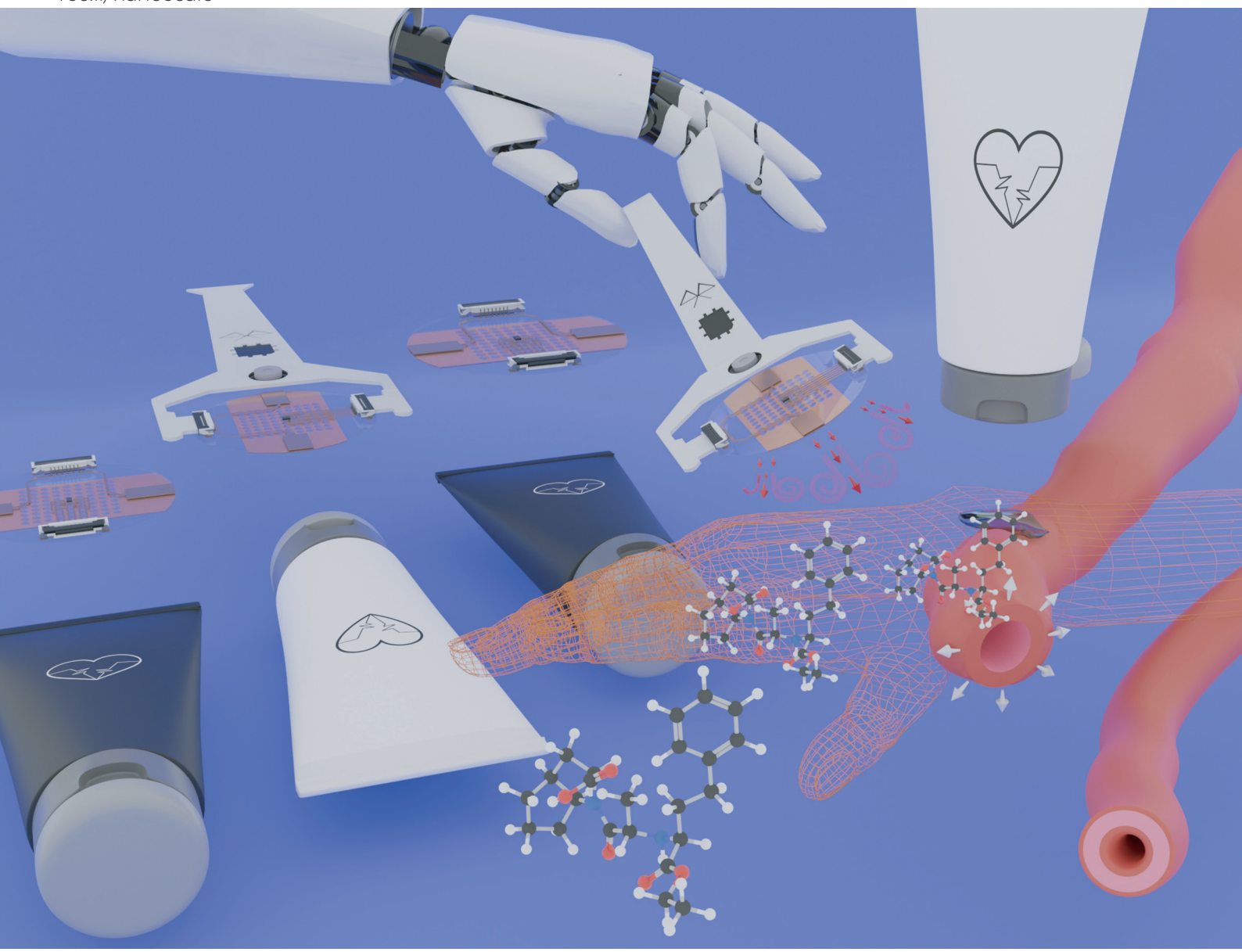

ISSN 2040-3372

ROYAL SOCIETY OF CHEMISTRY

PAPER
Sabine Szunerits *et al.*
Heat-based transdermal delivery of a ramipril loaded cream for treating hypertension

NCNST

Nanoscale

PAPER

View Article Online
View Journal | View Issue

Cite this: *Nanoscale*, 2022, **14**, 12247

Heat-based transdermal delivery of a ramipril loaded cream for treating hypertension†

Anna Voronova,[a] Quentin Pagneux,[a] Raphael Decoin,[b] Eloise Woitrain,[b] Laura Butruille,[b] Alexandre Barras,[a] Catherine Foulon,[c] Marie Lecoeur,[c] Diego Jaramillo,[d] José Rumipamba,[d] Sorin Melinte,[d] Amar Abderrahmani,[a] David Montaigne,[b] Rabah Boukherroub[a] and Sabine Szunerits *[a]

Received 26th April 2022,
Accepted 13th August 2022

DOI: 10.1039/d2nr02295h

rsc.li/nanoscale

Angiotensin-converting enzyme (ACE) inhibitors play an important role in the development of anti-hypertension approaches, with ramipril being one of the most widely used ACE inhibitor prodrugs orally administered once or twice a day. Due to its low bioavailability, large amounts have to be administered to obtain a therapeutic effect. In this work, we propose a ramipril loaded pharmaceutical formulation in contact with an electrothermal actuator based on a gold nanohole array as an efficient approach to increase the transdermal ramipril flux. Using rats as an *in vivo* model, the effect on the systolic and diastolic blood pressure is evaluated, showing that under optimized conditions the blood pressure could be regulated. Heat activation resulted in total drug delivery out of a bandage loaded with 1 mg ramipril, revealing a flux of 50.9 ± 2.8 μg cm^{-2} h^{-1}. Importantly, heat-based transdermal dispensing allowed efficient and rapid delivery of ramipril in spontaneously hypertensive rats, with its active form (ramiprilat) detected in blood as early as 5 minutes after delivery onset, accompanied by significant decrease in blood pressure.

1. Introduction

Hypertension plays a pivotal risk factor in cardiovascular diseases and is strongly influenced by environmental factors such as obesity, stress or smoking.[1,2] The angiotensin-converting enzyme (ACE), an important part of the renin–angiotensin system, converts angiotensin I into the vasoconstrictor angiotensin II and is responsible for the development of hypertension.[3] ACE inhibition became consequently an important therapeutic approach for the treatment of hypertension and prevention of cardiovascular diseases.[4–6] A handful of orally effective inhibitors of ACE have been described during the last decades.[7,8] The major differences between these therapeutics are related to pharmacokinetic properties and to the duration of anti-hypertension activity. Ramipril, a small molecular weight drug of 416.5 g mol^{-1}, remains one of the most widely used ACE inhibitor to treat high blood pressure and is prescribed after heart attack to help to prevent further strokes. This prodrug, used to improve membrane permeability of its corresponding active metabolite, ramiprilat,[9] is currently employed in a mono-therapeutic approach as well as in association with a thiazide-type diuretic.[10] Ramiprilat, formed by hydrolytic cleavage of the ester group of ramipril in the liver and in the kidney, has about six times ACE inhibitor activity of ramipril. The main issues of ramipril treatment are associated with its low oral bioavailability of 28–30% and a short biological half-life of 2–4 h. This differs from ramiprilat showing a bioavailability of 44% and a half-life around 13–17 h.[11,12] Depending on the pathology, ramipril is thus administrated orally once or twice a day to reach a total dose between 2.5 and 10 mg in adults exhibiting hypertension.

Next to the oral route, the transdermal drug delivery became one of the most widely considered alternative drug administration paths.[8,13,14] The advantages of skin-based drug delivery over oral as well parenteral administration is that this concept avoids the first pass metabolism, improves patient compliance with the ability to achieve relatively constant plasma drug levels over an extended period of time. Transdermal delivery of ACE inhibitors (*e.g.* captopril, trandolapril, lisinopril and perindopril, ramipril)[15–18] has been considered lately. Positive skin patch results have been reported for captopril, but the reported skin irritation has limited its utility in transdermal formulation.[19] The effect of topical ramipril formulation including stearic acid and stearic

[a]*Univ. Lille, CNRS, Centrale Lille, Univ. Polytechnique Hauts-de-France, UMR 8520 – IEMN, F-59000 Lille, France. E-mail: sabine.szunerits@univ-lille.fr*
[b]*Univ. Lille, Inserm, CHU Lille, Institut Pasteur de Lille, U1011 – EGID, F-59000 Lille, France*
[c]*Univ. Lille, CHU Lille, ULR 7365 – GRITA – Groupe de Recherche sur les formes Injectables et Technologies Associées, F-59000 Lille, France*
[d]*Institute of Information and Communication Technologies, Electronics and Applied Mathematics, Université catholique de Louvain, 1348 Louvain-la-Neuve, Belgium*
†Electronic supplementary information (ESI) available. See DOI: https://doi.org/10.1039/d2nr02295h

alcohol, glycerin, sodium dodecyl sulfate and paraffine was explored in a rat skin model.[18] This cream reduced scarring of wounds by reducing the expression of collagen I and III. Indeed, ramipril with an octanol/water partition coefficient[20] of 3.32, being only slightly above the optimal partition coefficient for transdermal delivery (considered to be 1–3),[21] is ideally adapted for the transdermal route. While several ramipril formulations have been proposed such as poly (amidoamine) dendrimer-based hybrid formulation,[10] or self-nanoemulsifying ramipril tablets,[22] the design of an efficient ramipril transdermal delivery system for the treatment of hypertension as exemplified in an *in vivo* model has not been considered in depth until now.

The purpose of this study was to evaluate the permeation performance for ramipril (1 mg) when loaded onto reduced graphene oxide (rGO) nanosheets as well as into a widespread transdermal vehicle used by compounding pharmacies, Pentravan® cream. An excised rat skin model was used to predict the permeation and the retention of the active compound in every skin layer. Enhanced ramipril permeation was observed upon combination with a nano-engineered heating element (Fig. 1). As shown previously by us, tuning the electrical resistivity of an array of gold nanoholes, patterned on polyimide, resulted in a fast-responding electrothermal skin patch for the controlled delivery of insulin *via* skin.[13] Heat has been validated to be a viable external trigger to enhance transdermal drug delivery of different therapeutics.[13,14,23–26] It is based mainly on heat-assisted microporation to create transport channels in the skin, which allows enhanced drug delivery.[27] We show here that ramipril loaded onto rGO and heat activated provides a ramipril flux equal to 26.9 ± 3.8 μg cm^{-2} h^{-1} independent of the heating approach chosen, photothermal or electrothermal. By replacing rGO by Pentravan® cream as drug reservoir, under heat activation, an almost complete ramipril delivery is achieved with a flux as high as 50.9 ± 2.8 μg cm^{-2} h^{-1} from 1 mg ramipril-loaded cream.

2. Results and discussion

2.1. Heat-based transdermal delivery of ramipril loaded onto reduced graphene oxide (rGO/ramipril)

We have shown in several works the interest of using reduced graphene oxide (rGO) nanosheets for loading drugs followed by thermal release and notably controlled delivery across the skin at demand.[13,14,25,26] Two different approaches were implemented based on either photothermal[14,25,26] or electrothermal heating.[13] As near-infrared (NIR) light can penetrate up to 10 μm into soft tissues,[28] the combination with NIR absorbing materials such as rGO is beneficial for enhanced transdermal drug delivery. Ramipril can be easily loaded onto rGO nanosheets by π–π stacking, hydrogen-bonding and/or van der Waals interactions. The loading capacity of rGO for ramipril, as determined by measuring the concentration of ramipril before and after loading using high performance liquid chromatography (HPLC), indicates that a total ramipril loading is obtained using a rGO/ramipril ratio of 5 (*e.g.* 5 mg rGO and 1 mg ramipril) (Fig. 2a). This is an important finding, as depending on the pathology, total ramipril administration doses are in the milligram range.

Deposition of rGO/ramipril onto a flexible bandage, in our case a poly(imide) film (*e.g.* Kapton), and illumination with a laser at 980 nm (500 mW cm^{-2}) shows a steadily increase in temperature, reaching 38 ± 2 °C after 10 min (Fig. 2b). The temperature increase could be improved (increase to 50 ± 2 °C after 10 min) by depositing the same mixture onto a Kapton

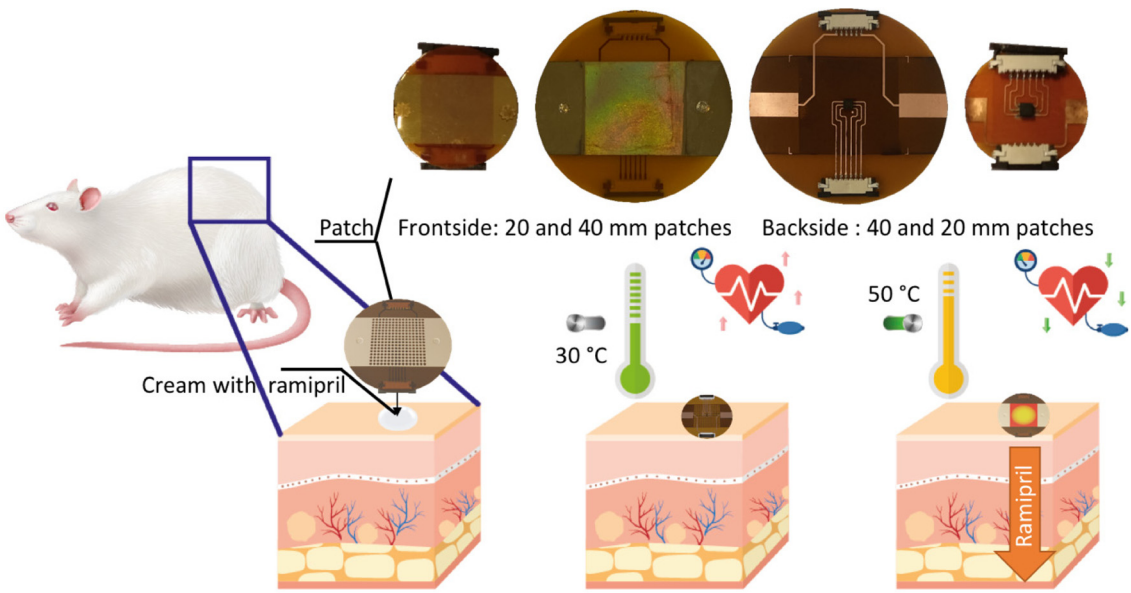

Fig. 1 *In vivo* model for electrothermal ramipril delivery. Enhanced ramipril permeation upon combination of nano-engineered heating elements with a transdermal vehicle, Pentravan® loaded with ramipril (10%).

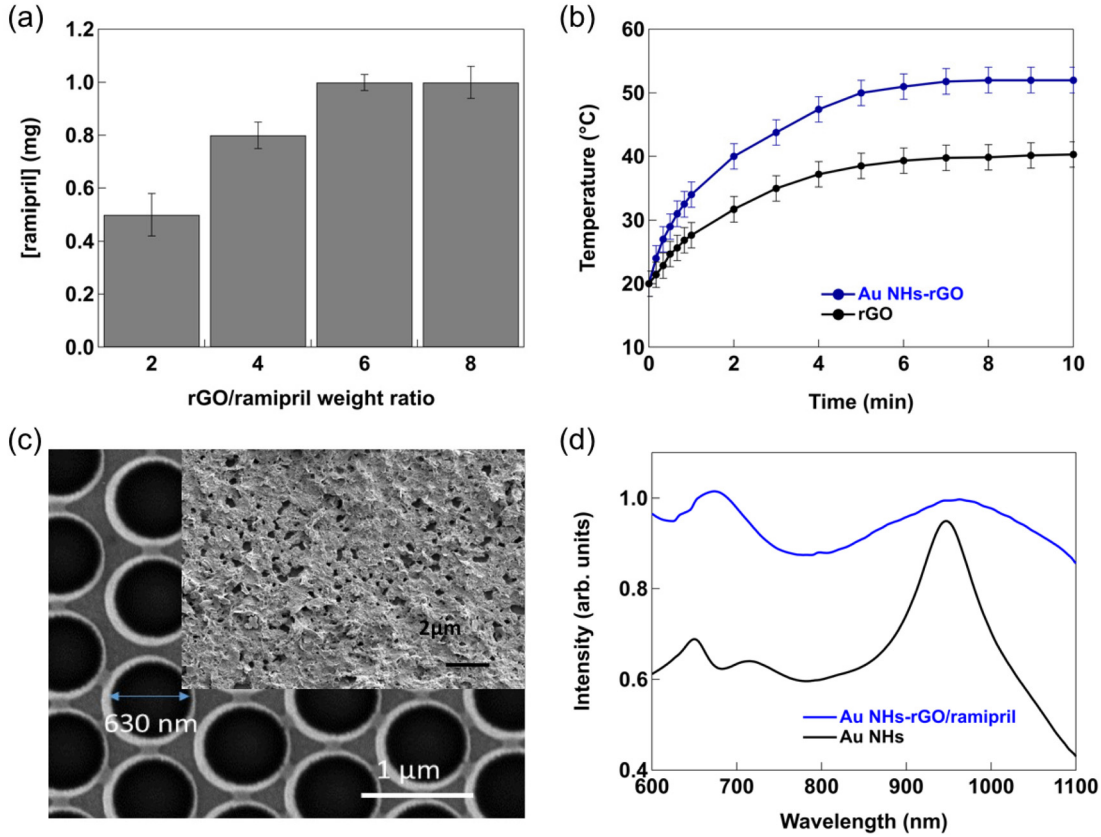

Fig. 2 Ramipril loading onto rGO-coated nano-heating elements. (a) Ramipril (1 mg) loading capacity of rGO as a function of rGO/drug ratio. (b) Photothermal heating curves of water using rGO directly deposited on Kapton or on a nano-heater in the form of Au NHs. (c) SEM image of Au NHs without and upon coating with rGO/ramipril (inset). (d) UV-Vis absorption spectra of Au NHs and Au NHs-rGO/ramipril in air.

thin film modified by colloidal lithography with a 40 nm thick gold nanoholes array of 630 ± 10 nm in diameter with a center-to-center spacing of 980 nm (Fig. 2c). The nano-heater surface shows a strong absorption maximum at 980 nm due to the excitation of surface plasmon waves in the substrate, acting as two-dimensional diffraction gratings that convert incident photons into SP waves (Fig. 2d). Post-coating of the Au NHs heater with rGO/ramipril mixture by drop-casting results in a Au NHs device entirely covered with rGO nanoflakes of about 10–1000 nm in thickness (inset Fig. 2c) with a synergetic effect on the absorption intensity, and broadening of the plasmonic band (Fig. 2d).

While the temperature increase of the photothermal heating approach is comparable to the electrothermal one (Fig. 2b and 3a) when 1.0 V is applied, the time-scale of photothermal heating differs largely from the electrothermal heating. The electrothermal activation results in an almost instantaneous increase of the temperature as well as a sharp decrease once the voltage bias is interrupted (ESI, Fig. S2–S5†).

The biocompatibility of rGO-coated nano-heating elements was assessed on the HeLa cell line (see ESI, Fig. S1†) using the resazurin assay, based on the conversion of non-fluorescent dye to a fluorescent molecule by mitochondrial and cytosolic enzymes. No loss in cell viability and metabolic activities was observed upon incubation of the rGO-coated nano-heaters for 24 h. Photothermal or electrothermal activation for 10 min did not result in any cell damage either.

To determine the influence of electrothermal and photothermal activation on the flux of ramipril through skin, permeation studies were performed using rat skin (Fig. 3b). Fig. 3b shows the percentage of permeated ramipril over 24 h, passively and when heat activated for 10 min from a formulation containing 1 mg ramipril. After 24 h in the case of the thermal activation about 50% of the ramipril loaded onto rGO had permeated the skin.

The flux of ramipril, determined from the cumulative ramipril amount *versus* time curves, is displayed in Fig. 3c; a passive flux of 12 ± 2 μg h^{-1} was recorded, which increased to 21 ± 3 μg h^{-1} and 22 ± 2 μg h^{-1} under photothermal and electrothermal activation, respectively. Considering the surface area of the Franz diffusion cell of 0.78 cm^2, passive and heat-activated ramipril fluxes equal to 15.4 ± 2.5, 26.9 ± 3.8 and 28.2 ± 2.6 μg cm^{-2} h^{-1} were involved. Aiming at a daily dose of 1 mg would require a delivery bandage of about 1.5 times the current size, something which can be easily achieved. From the HPLC analysis of the permeated ramipril (Fig. 3d), it appears that ramipril has not been degraded during the skin

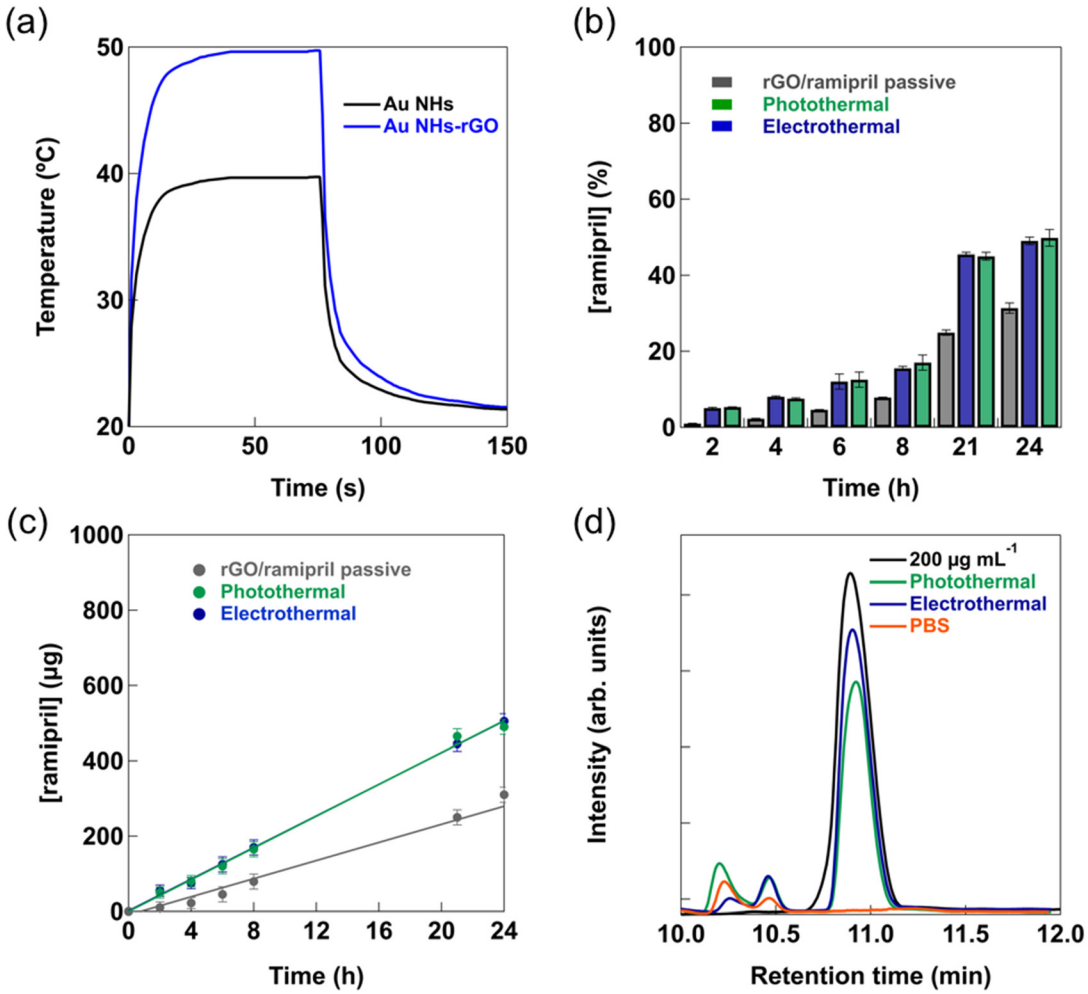

Fig. 3 Permeation of ramipril passively and under heat activation. (a) Temperature profiles over time upon the application of 1.0 V voltage bias on Au NHs and on Au NHs/-rGO bandages. (b) *Ex vivo* permeation profiles of rGO-nanhoheaters loaded with ramipril (1 mg in 1 mL of water) through rat skin either passively (black) or *via* photothermal (green) and electrothermal (blue) activation for 10 min (n = 3). (c) Permeation profile of ramipril as a function of time. (d) HPLC profiles of ramipril (200 μg mL^{-1}) before and after skin permeation under either photothermal (1 W cm^{-2}) or electrothermal (1.0 V) activation for 10 min. In a control experiment, PBS was permeated and the solution was analyzed. Error bars (n = 3) represent standard error of the mean (SEM).

permeation process. Next to the ramipril peak at 10.89 min, peaks at 10.20 and 10.45 min are observed. In a control experiment using only PBS, the peaks at 10.20 and 10.45 min are also present in a different intensity ratio than in the case of the electrothermal release experiment, with the peak at 10.20 min being less pronounced than that at 10.45 min. These peaks remained unassigned and are most likely related to skin released material.

2.2. Heat-based transdermal delivery of ramipril loaded into Pentravan® cream

As shown until now, the advantage of using rGO/ramipril as transdermal formulation is linked to the dual character or rGO: (i) being a photothermal agent as well as a good heat conducting matrix (the affinity between rGO and aqueous solutions of ramipril is decreased upon application of a photothermal or electrothermal ramp, resulting in drug release and transdermal delivery) and (ii) working as a drug reservoir. However, only about half of the integrated ramipril is thermally released from the rGO matrix. To overcome this limitation, a Pentravan® cream was used instead of the rGO reservoir. In addition, it was employed together with ramipril in a Pentravan®/ramipril ratio of 9/1. Fig. 4a shows that after 24 h more than 50% had been transdermally delivered using the Pentravan®-ramipril formulation passively. Heat activation however resulted in an almost total drug permeation with a ramipril flux under heat-based conditions of 50.9 ± 2.8 μg cm^{-2} h^{-1}. Similar results were reported for skin delivery of captopril from a range of cellulose-based gels using capric acid as a skin permeation enhancer.[29] The results indicate that the photothermal activation approach and the electrothermal method behave the same for skin permeation of the drug. The main difference between these approaches is that the optical based photothermal drug delivery concept has a specific pene-

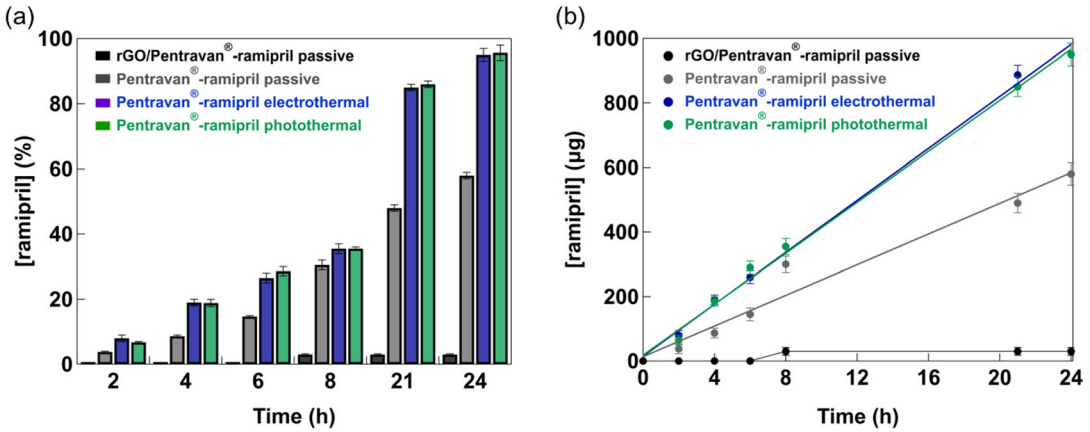

Fig. 4 Transdermal ramipril delivery from Pentravan® cream formulations. (a) *Ex vivo* permeation profiles of Pentravan® cream loaded with ramipril (ratio of 9/1) through rat skin either passively (grey) or *via* photothermal (green) or electrothermal (blue) activation for 10 min (n = 3). The control is the rGO-coated nanoheater with the Pentravan®-ramipril formulation and not activated (black). (b) Permeation profiles of ramipril as a function of time (n = 3). Error bars represent standard error of the mean (SEM).

tration depth into the skin tissue, while electrothermal heating is a contact surface-induced approach. The advantage of an electrothermal drug induced release is thus mainly based on easier partial implementation as wearable technology with low power density consumption. Currently, a portable optical system would be required in the photothermal strategy, while simple, rechargeable battery-enabled electronics can activate the electrothermal bandage allowing a better integrated and miniaturized device construct.

Before further testing the Pentravan®-ramipril formulation in *in vivo* models, the biological activity of ramipril that has crossed the skin, *i.e.* ACE inhibition, was assessed using the angiotensin I converting enzyme activity assay. The assay is based on a synthetic fluorogenic substrate that, when cleaved by ACE, forms a fluorescent compound detectable by its fluorescence at 405 nm. Activity of ACE was measured alone and with solutions prepared from the receptor compartment solution collected 24 h after the beginning of the transdermal kinetic study upon heating activation. According to the experimental protocol, the receptor compartment solution was finally 10 000-fold, 1000-fold and 100-fold diluted in a mixture containing ACE and its substrate (ESI, Fig. S6†). Increasing inhibition rates of 28.5 ± 8.5%, 85.4 ± 1.9% and 99.0 ± 1.0% were respectively measured. This result demonstrates that ramipril stays active, *i.e.* inhibits ACE, even after skin permeation using thermal activation.

2.3. *In vivo* experiments using a hypertensive rat model

To clearly address the question of the ability of the developed approach to regulate hypertension and to determine the amount of ramipril entering the blood stream, a well-established hypertensive animal model, the salt-fed spontaneous hypertensive (SHR) rat model, was used.[30] Information about the pharmacokinetics of the cream formulation in hypertensive rats was obtained by determining the blood level of ramipril and ramiprilat after application of Pentravan®-ramipril formulation containing 1 mg of ramipril prodrug over an area of about 1 cm^2. From liquid chromatography/mass spectrometry LC/MS analysis (Fig. 5a) of serum collected after a 1 mg ramipril administration *via* gavage, it becomes clear that the prodrug is indeed completely converted into the physiological active form, ramiprilat with a retention time of 9.5 min (green); ramipril could not be detected in the blood serum after 4 h (orange). As seen in Fig. 5b, quantitative levels of ramiprilat could be detected in the blood stream of the rat after gavage, leveling off after 40 min up to 300 ng mL^{-1}. Ramiprilat reached peak concentrations of 33.5 ± 8.9 ng mL^{-1} in serum after 1 h under electrothermal heat (1 V) activation for 10 min (Fig. 5c). Ramiprilat levels decreased to 23.8 ± 2.8 ng mL^{-1} after 3 h. In comparison, ramiprilat reached only peak concentrations of 26.4 ± 8.9 ng mL^{-1} in serum after 2 h under passive condition and decreased thereafter. As photothermal and electrothermal heating approaches provided comparable transdermal ramipril flux, *in vivo* testing was restricted to electro-thermal activation in line with the reduction of the number of animals used in the study. Since the skin was exposed to external heat, it was necessary to evaluate any tissue structure changes caused by electrothermal activation. Fig. 5d depicts the histological analysis of rats' skin in contact with the ramipril loaded cream before and after heat activation using conventional hematoxylin and eosin (H&E) staining. No visible effect of electrothermal heat on skin structure was observed in comparison with initial, non-treated skin and skin covered with Pentravan®-ramipril cream without heat activation.

The SHR rats presented significant elevated blood pressure at baseline (systolic blood pressure: 207 ± 2 mmHg, diastolic blood pressure: 186 ± 3 mmHg – n = 3 – data not shown), as expected from literature data.[30] Under slight isoflurane anesthesia, 4 h transdermal ramipril delivery from Pentravan® cream significantly decreased systolic blood pressure, while transdermal vehicle delivery was ineffective under these con-

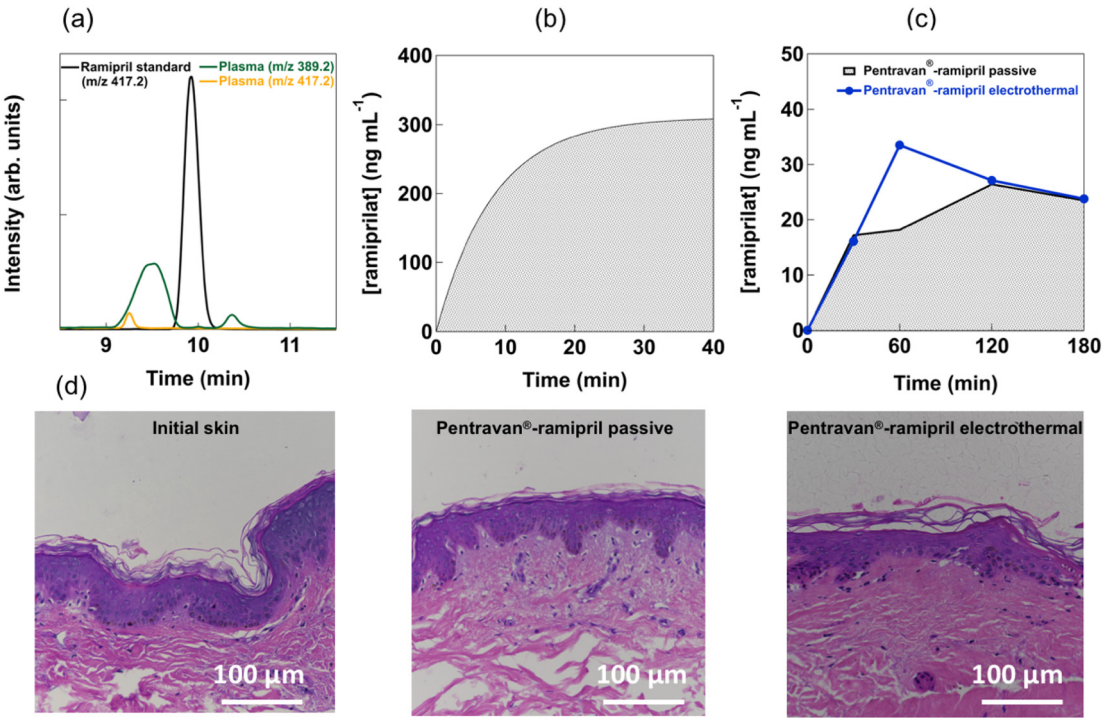

Fig. 5 Pharmacokinetics of Pentravan®-ramipril formulation in hypertensive rats. (a) LC/MS chromatograms of serum from rats treated with 1 mg of ramipril *via* gavage using selective ion monitoring (SIM) mode at *m/z* 389.2 $[M + H]^+$ (ramiprilat) and at *m/z* 417.2 $[M + H]^+$ (ramipril). (b) Dose–response curve of ramiprilat detected in the blood stream of rats administered with 1 mg of ramipril *via* gavage, as determined by LC/MS (n = 3). Results are expressed as mean ± SEM. (c) Dose–response curve of ramiprilat in blood stream of Pentravan® cream loaded with ramipril (1 mg) under passive condition and electrothermal heat (1.0 V) activation for 10 min (n = 3). Results are expressed as mean ± SEM. (d) Bright-field micrograph images of histological section of rat skin before and after contact with Pentravan®-ramipril formulation (12 h) as well as after electrothermal activation for 10 min at 1.0 V.

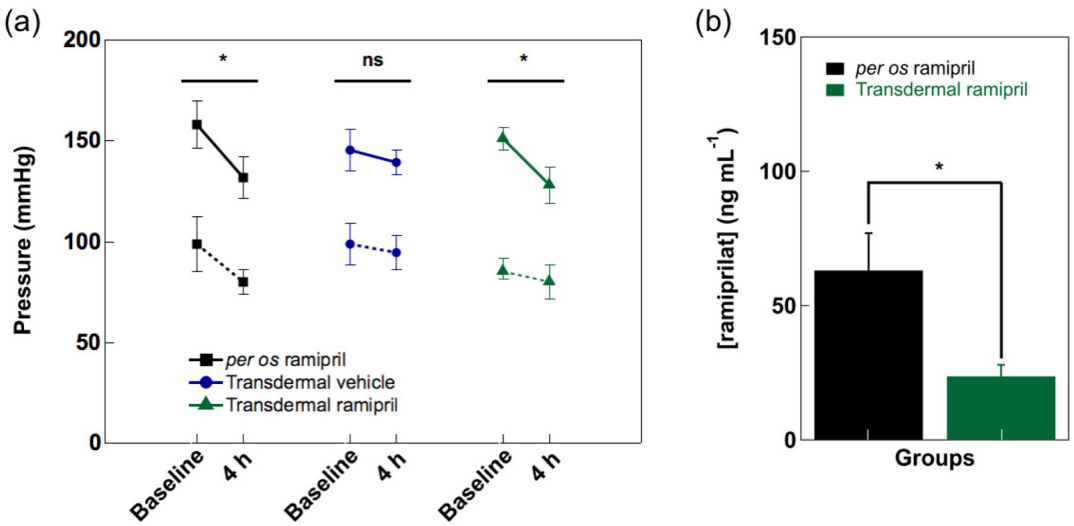

Fig. 6 *In vivo* studies using SHR rats. (a) Systolic and diastolic blood pressures in hypertensive rats were measured by tail cuff method at baseline and 4 h after compounds administration. Measurements were performed under isoflurane anesthesia (n = 6 per group). Results are expressed as mean ± SEM. Continuous lines represent changes in systolic blood pressure; dotted lines indicate changes in diastolic blood pressure. *Post-hoc* paired-*t* tests, *$p < 0.05$. (b) Quantification of ramiprilat detected in the blood stream of rats administered with 3 mg kg^{-1} of ramipril *via* gavage or *via* transdermal delivery, 4 h after compounds administration, as determined by LC/MS (n = 5 per group). Results are expressed as mean ± SEM. Unpaired-*t* tests, two-tailed, *$p < 0.05$.

ditions (Fig. 6a). *Per os* administration of ramipril (3 mg kg^{-1}), used as a positive control, successfully reduced systolic blood pressure after 4 h of drug intake. Note that a slight decrease in diastolic blood pressure was also observed in both *per os* and transdermal ramipril administration groups (3 mg kg^{-1}) without reaching statistical significance. After 4 h ramipril administration, ramiprilat could still be detected in blood serum at a concentration of 63.2 ± 15.6 ng mL^{-1} and 23.8 ± 4.8 ng mL^{-1} *via* gavage or under electrothermal heating, respectively (Fig. 6b). Taken together, these data indicated that transdermal ramipril delivery was effective in reducing blood pressure in the SHR model.

3. Conclusion

In conclusion, the ACE inhibitor ramipril loaded into Pentravan® cream enhanced overall transdermal delivery properties under heat activation. Considering the typical daily oral delivery dose of 1–2 mg, a formulation containing 1 mg of the prodrug was considered. No skin irritation was observed for the formulation as no skin penetration enhancers were used for an efficient delivery. Under stationary heat gradient conditions, a ramipril flux of 50.9 ± 2.8 μg cm^{-2} h^{-1} was measured that corresponds to a sufficient daily dose of 1.22 ± 0.067 mg. Using spontaneously hypertensive rats, the physiological effect of transdermal administered ramipril was evaluated. The systolic and diastolic blood pressure initially measured as 207 ± 2 mmHg and 186 ± 3 mmHg, respectively, showed a significantly decreased systolic blood pressure after 4 h, while the transdermal vehicle delivery alone was ineffective at this time scale. Taken together, these data showed that transdermal ramipril delivery was effective in reducing blood pressure in the SHR model. These findings highlight the potential of this approach for the management of patients with chronic hypertension as an alternative over oral administration.

4. Experimental section

4.1. Materials and methods

Ramipril was obtained from Sigma-Aldrich (France). Ramiprilat (RAMT, $C_{21}H_{28}N_2O_5$, monoisotopic mass: 388.1998, purity ≥98%) was obtained from Cayman Chemical (Ann Arbor, MI, USA). Phosphate buffered saline (PBS, pH 7.4), ethanol (EtOH), Dulbecco's modified Eagle's medium (DMEM), dimethylsulfoxide (DMSO), LC/MS grade methanol, 0.1% formic acid in water (v/v), and 0.1% formic acid in acetonitrile (v/v) were purchased from Fisher Scientific SAS (Illkirch, France). Graphene oxide (GO) was obtained from Graphenea (Spain). Kapton® NH polyimide foils were provided by DuPont (Circleville, OH, USA). Pentravan® cream was purchased from Fagron, Inc. (USA).

The nano-element heaters were fabricated as reported previously.[13] Briefly, Kapton® HN polyimide foils (cut in circular pieces with 20 or 40 mm diameter and backside Cu patterned) were cleaned with acetone in an ultrasonic water bath for 30 min, followed by isopropanol for 10 min and then dried under a nitrogen flow. A monolayer of 980 nm polystyrene beads (Microparticles GmbH) was first deposited in the center of the Kapton patch, frontside, with an area of 11 × 11 or 20 × 20 mm^2 by self-assembly. To reduce the size of the particles, SF_6 and oxygen plasma etching was employed (6 mTorr). The samples were coated with 2 nm Ti followed by 40 nm Au at a constant deposition rate of 1 Å s^{-1} using physical vapor deposition. The polystyrene beads on top of the Kapton were removed by dissolution in chloroform (overnight). To facilitate the application of the bias voltage, 2 nm Ti and 40 nm Au contacts were further deposited on the patches and connected on the backside of the devices *via* flat flexible connectors (FFCs) and FFC jumper cables. Electrical power has been supplied with AA batteries (see ESI†) and electronic boards were used for both wireless control and bias voltage calibration.

4.2. Instrumentation

Scanning Electron Microscopy (SEM) images were obtained using an electron microscope ULTRA 55 (Zeiss) equipped with a thermal field emission emitter and three different detectors (Energy selective Backscattered Detector with filter grid, high efficiency In-lens Secondary Electron Detector and Everhart–Thornley Secondary Electron Detector). UV-Vis absorption spectra were recorded using a PerkinElmer Lambda UV-Vis 950 spectrophotometer. The wavelength range was 600–1100 nm. The photothermal properties were assessed using a 980 nm-continuous wave laser (Gbox model, Fournier Medical Solution) with an output light at 980 nm at various power densities. This laser was injected into a lens and placed at 10.5 cm from the bottom of the wells. The resulting beam divergence allowed to illuminate uniformly a surface of 1 cm^2. The temperature changes on the surface of the patch were captured by an infrared camera (FLIR A655sc) and treated using FLIR ResearchIR Max software; the readings corresponded to thermal sensors integrated to the backside of the patches.

4.3. Loading of reduced graphene oxide (rGO) nanosheets with ramipril

rGO was prepared by adding hydrazine hydrate (0.50 mL, 32.1 mM) to 5 ml of graphene oxide (GO) aqueous suspension (0.5 mg mL^{-1}) in a round bottom flask and heated in an oil bath at 100 °C for 24 h. During this time, the reduced GO gradually precipitates out of the solution. The product was isolated by filtration over a polyvinylidene difluoride membrane with a 0.45 mm pore size, washed copiously with water (5 × 20 mL) and methanol (5 × 20 mL), and dried in an oven at 60 °C for 6 h. An aqueous suspension of rGO (5 mg mL^{-1}) and ramipril (1 mg mL^{-1}) was drop-casted onto Kapton or Kapton/Au NHs and allowed to dry over night at 70 °C.

4.4. Formulation of ramipril loaded Pentravan® cream

Ramipril was formulated in Pentravan® with 10% (w/w) EtOH. The ratio between cream and ramipril was 9/1 with a drug content of 1 mg. Each formulation was prepared by dispersing

a weighed amount of ramipril in ethanol using sonication for 15 min. The transdermal vehicle was added to the suspension and the formulation was vortexed thoroughly at 800 rpm for 15 min using a nickel-stainless steel microspatula with a flat end (40 × 6 mm^2) (VWR International, Fontenay-sous-Bois, France) which tip was bent at an angle of 90°.

4.5. Transdermal permeation experiments using an *ex vivo* rat skin model

Skin permeation studies were performed using fresh rat skin. SHR rats were anaesthetized with isoflurane, shaved with an electric shaver (Philips Series 7000) and further treated with a depilatory cream (Veet) for 1.5 min. Then the rats were killed by cervical dislocation and the skin from the back of the rat was cut into pieces of at least 20 mm in diameter and preserved in Dulbecco's modified Eagle's medium (DMEM). Static Franz diffusion cells (Proviskin, France), exhibiting an effective area of 0.785 cm^2, were used for skin permeability tests. After filling the receptor compartment (8 mL) with degassed phosphate buffered saline (PBS 1×, pH = 7.4), the solution was maintained at 37 °C using a circulating bath (Julabo) and stirred with a magnetic stirring bar at around 500 rpm. Freshly cut rat skin was clamped between the donor and the receptor compartments and pre-incubated for 20 min. The rGO-ramipril loaded patch and ramipril loaded Pentravan® cream coated electrothermal patch were applied on the top of the skin. Passive permeability as well as photothermal (980 nm, 1 W cm^{-2}) and electrothermal enhanced (1.0 V, 10 min) permeability were evaluated. At determined time intervals, 300 µL aliquots of diffused solution were removed from the receptor compartment and analysed by HPLC. After each sampling, an equal volume of fresh diffusion medium was added to the receptor compartment to maintain a constant volume. All experiments were performed in triplicate.

The ramipril flux (J, µg h^{-1} cm^{-2}) was calculated using equation $J = m/A$, with m being the linear slope of the cumulative ramipril amount *versus* time curves at equilibrium (µg h^{-1}), and A the surface of the membrane of the Franz cell (0.785 cm^2).

4.6. Quantification of permeated ramipril

Analysis was performed by high performance liquid chromatography (HPLC) using a Shimadzu LC2010-HT system (Shimadzu, Tokyo, Japan). Ramipril was separated on a 5 µm C18 AQ Uptisphere X®, 250 mm × 4.6 mm column (Interchim, Montluçon, France) heated to 40 °C. The mobile phase consisted of a mixture of eluent A (formic acid 0.1% in water) and eluent B (formic acid 0.1% in acetonitrile) at a flow rate of 1 mL min^{-1}. The samples were injected at a volume of 40 µL and the detection was at a wavelength of 215 nm.

4.7. Quantification of ramipril and/or ramiprilat in plasma

The LC 1260 Infinity II system (Agilent Technologies France, Les Ulis, France) equipped with a quaternary pump (G7111), a thermostated column compartment (G7116A), an autosampler (G7129), and a variable wavelength detector (G7114) was coupled to an Agilent G6125BW single-quadrupole mass spectrometer (SQ/MSD) and was operated with an ESI/APCI multimode source (G1978B). An Agilent OpenLAB ChemStation was used for the control of the equipment, data acquisition, and analysis.

The separation was performed on a 5 µm C18 AQ Uptisphere X®, 250 mm × 4.6 mm column (Interchim, Montluçon, France). The mobile phase used was a mixture of water with 0.02% formic acid (v/v) (A) and acetonitrile with 0.02% formic acid (v/v) (B) and the flow rate was set at 0.8 mL min^{-1}. Gradient elution was employed and was used as follows: 5% B during 0.5 min, 5 to 95% B from 0.5 to 10.5 min, 95% B from 10.5 to 15 min, 5% B at 15.01 min and 6 min re-equilibration at 5% B. The column temperature was set at 35 °C, and the injection volume was 20 µL.

Electrospray ionization (ESI) in the positive ion mode was used as the ionization source. Nitrogen was used as the nebulizer drying gas and was maintained at a flow of 5 L min^{-1} with a nebulizer pressure of 60 psi. The drying gas temperature was set at 250 °C and the capillary voltage was 2000 V. The vaporizer temperature was set at 150 °C and the charging voltage was 2000 V. The fragmentor voltage was set at 120 V. Chromatograms were obtained using selective ion monitoring (SIM) mode at m/z 417.2 for ramipril ($[M + H]^+$), and m/z 389.2 for ramiprilat ($[M + H]^+$), with these optimized values.

Ramipril and ramiprilat were accurately weighed and dissolved in DMSO to obtain 1 mg mL^{-1} standard stock solutions. Standard stock solutions were stored at 4 °C when not in use. Working standard solutions were prepared daily by dilution in 50/50 water/methanol (v/v) from stock solutions to create the necessary concentrations. The calibration curves were established using eight calibration standards prepared by spiking blank rat plasma with the working solutions, to reach the final concentrations of 25, 50, 100, 200, 400 and 800 ng mL^{-1}.

The rat plasma samples were taken out from the freezer and thawed at room temperature. A 100 µL aliquot of a rat plasma was taken into a 1.5 mL polypropylene tube and 300 µL of cold methanol was added to precipitate the plasma protein, and then vortexed for 15 s. The spiked samples were placed at −20 °C for 15 min and were centrifuged at 15 000g and at 4 °C during 15 min. The supernatants were filtered through 0.22 µm RC membrane and put into the autosampler sample bottles for analysis by the LC/MS system.

4.8. *In vitro* activity of ramipril after skin crossing

Activity of ramipril that crossed the skin (ACE inhibition), after application of ramipril loaded Pentravan® cream using thermal activation, was evaluated by fluorometric measurement using the angiotensin I converting enzyme activity assay kit supplied by Sigma-Aldrich (Saint Quentin Fallavier, France). The assay is based on the use of a synthetic fluorogenic substrate, cleaved by ACE to form a fluorescent compound. Fluorescence measurements (n = 3) were performed on a Varioskan Flash (ThermoFisher Scientific, Courtaboeuf, France), at 37 °C, using a 96-well black plate, with excitation and emission wavelengths set at 320 nm and 405 nm, respectively.

Firstly, fluorescence of eight calibration standards, containing the fluorescent compound with concentrations ranging from 0 to 0.8 nM was measured. Secondly, ACE activity was determined alone or in mixture with receptor compartment solution. To this purpose, different solutions were prepared: (1) blank: assay buffer; (2) positive control: ACE solution in assay buffer and (3) inhibitor assay: receptor compartment solution, at 24 h after permeation beginning, diluted in ACE solution (5000-fold factor; 500-fold factor and 50-fold factor). ACE concentration was equal in solutions (2) and (3). A volume of 50 μL of each solution was introduced in the multiwell plate, brought to 37 °C for 5 min and then mixed with 50 μL of a substrate solution prepared in the assay buffer. The fluorescence of the resulting solution was measured every minute for 5 min. Fluorescence of the blank sample was subtracted to fluorescence values of solutions (2) and (3). The ACE activity was calculated in several steps: (i) determination of the slope of the curve describing the fluorescence measured *versus* the fluorescent product concentration by linear regression for standard solutions ($Slope_{standard}$, RFU $nmol^{-1}$); (ii) determination of the slope of the kinetic curve relying the fluorescent measured for positive control and inhibitor solutions *versus* time, by linear regression ($Slope_{sample}$, RFU min^{-1}); (iii) determination of the ACE activity (nmol min^{-1} or mU) equal to the ratio $Slope_{sample}/Slope_{standard}$. Finally, the inhibition rate was estimated as follow:

$$\text{Inhibition rate}\,(\%) = 100 \times \frac{\text{Activity}_{\text{without inhibitor}} - \text{Activity}_{\text{with inhibitor}}}{\text{Activity}_{\text{without inhibitor}}}.$$

4.9. *In vivo* delivery of ramipril in spontaneously hypertensive rats

In vivo delivery of ramipril from Pentravan® cream was investigated in spontaneously hypertensive (SHR) rats as a model. 3 groups of rats were studied: (i) force-feeding with ramipril solution (3 mg mL^{-1}) as a control, (ii) Pentravan® cream with electrothermal activation and (iii) 10% ramipril containing Pentravan® cream with electrothermal activation. The day before the experiment, the back of the rats was shaved (Philips Series 7000) and treated with a depilatory cream (Veet) for 1.5 min to eliminate all the remaining hair. Each rat was weighted (400 ± 12 g) in order to calculate the amount of cream and ramipril solution that has to be used. For the cream experiments, before its deposition, the rats were anesthetized with isoflurane for 3 min. After, 12 mg of Pentravan® cream or ramipril containing Pentravan® cream were applied to the shaved back area of the rat and covered with electrothermal patch that was fixed with the help of adhesive tape (Sparadrap Micropore, 2133). The patch was activated for 10 min to reach 52 °C under anesthesia and then removed. For the force-feeding experiments, 400 μL of 3 mg mL^{-1} ramipril solution were orally administrated to the rats without anesthesia using the oral gavage feeding needle. All animal experiments throughout this study were conducted according to the policy of the Federation of European Laboratory Animal Science Association and the European Convention for the protection of vertebrate animals used for experimental and other scientific purposes, with implementation of the principle of the 3Rs (replacement, reduction, refinement). Animal procedures were performed in accordance with the Guidelines for Care and Use of Laboratory Animals of CHU Lille and experiments were approved by the Animal Ethics Committee of CHU Lille. The work runs under protocol number APAFIS#26534-2020060414283744 v6.

SHR rats were assigned to one of the 3 following groups: ramipril *per os*; transdermal vehicle; transdermal ramipril. Animals in each group served as their own control. Basal blood pressure and heart rates were measured at baseline and 4 h after treatments, under isoflurane anesthesia (2.0% isoflurane, oxygen flow rate 800 mL min^{-1}). Blood pressure was measured by the tail-cuff method using non-invasive blood pressure (NIBP) measuring apparatus (IN125, AD Instruments, Australia). Recordings and analysis were realized by using Power Lab data acquisition system and computer running Lab Chart software (PowerLab26T PL26T04Ad Instruments, Sydney, Australia). Blood was collected by tail, using a needle 21G and drop in Microvette® EDTA- (Sarstedt). Blood was kept on ice during all experiments, and then centrifuged (10 min at 10.000*g*) to remove blood cells. The plasma samples were kept at −80 °C until use. For determination of ramipril and ramiprilat activity, the blood sampling was realized before medication and after 4 h.

4.10. Skin staining and imaging

For tissue section, skin samples were first fixed in 4% paraformaldehyde (Sigma, France) for 48 h and embedded in paraffin using Spin tissue processor STP120 (Thermo Scientific, France) and tissue embedding station Leica EG1160 (Leica, France). Samples were then sectioned into 5 μm-thick slices using a rotary microtome Leica RM2145 (Leica, France). Finally, the slices were fixed on glass slides by heating. After deparaffinization, the tissue sections were stained with Hematoxylin & Eosin stain kit (Vector Laboratories, France) to observe the tissue structure. Samples were investigated using a Nikon Eclipse Ti2-U Inverted Microscope System (Nikon, France) using a CFI PLAN APO -LAMBDA 20X 0.75/1 mm CO/0.17 objective. Images were captured using a Nikon DS-Ri2 microscope camera (Nikon, France) for histological observations through NIS-Elements Microscope Imaging.

Conflicts of interest

There are no conflicts to declare.

Acknowledgements

AV thanks the I-SITE ULNE Foundation for a PhD fellowship. DM, RD, LB and EW are supported by grants from Agence

Nationale pour la Recherche (ANR-10-LABX-0046, ANR TOMIS-Leukocyte: ANR-CE14-0003-01 and ANR CALMOS: ANR-18-CE17-0003-02), the Leducq Foundation LEAN Network 16CVD01 and the National Center for Precision Diabetic Medicine – PreciDIAB (ANR-18-IBHU-0001; 20001891/NP0025517; 2019_ESR_11). This work has received funding from the European Union's Horizon 2020 research and innovation programme under Grant Agreement No. 956923.

References

1 R. M. Carey, P. Muntner, H. B. Bosworth and P. K. Whelton, *J. Am. Coll. Cardiol.*, 2018, **72**, 1278–1293.
2 B. Williams, G. Mancia, W. Spiering, E. Agabiti Rosei, M. Azizi, M. Burnier, D. L. Clement, A. Coca, G. De Simone, A. Dominiczak, T. Kahan, F. Mahfoud, J. Redon, L. Ruilope, A. Zanchetti, M. Kerins, S. E. Kjeldsen, R. Kreutz, S. Laurent, G. Y. H. Lip, R. Mcmanus, K. Narkiewicz, F. Ruschitzka, R. E. Schmieder, E. Shlyakhto, C. Tsioufis, V. Aboyans, I. Desormais and E. S. D. Group, *Eur. Heart J.*, 2018, **39**, 3021–3104.
3 L. M. Burrell, C. I. Johnston, C. Tikellis and M. E. Cooper, *Trends Endocrinol. Metab.*, 2004, **15**, 166–169.
4 A. Goyal, A. S. Cusick and B. Thielemier, *ACE Inhibitors*, StatPearls Publishing, Treasure Island, 2022.
5 T. Ghatage, S. G. Goyal, A. Dhar and A. Bhat, *Hypertens. Res.*, 2021, **44**, 740–755.
6 K. Hanif, H. K. Bid and R. Konwar, *Hypertens. Res.*, 2010, **33**, 11–21.
7 J. Doane and B. Stults, *J. Clin. Hypertens.*, 2013, **15**, 230–233.
8 L. B. Arendse, A. H. J. Danser, M. Poglitsch, R. M. Touyz, J. C. Burnett, C. Llorens-Cortes, M. R. Ehlers and E. D. Sturrock, *Pharmacol. Rev.*, 2019, **71**, 539–570.
9 D. G. Levitt and R. C. Schoemaker, *BMC Clin. Pharmacol.*, 2006, **6**, 1.
10 M. K. Singh, D. Pooja, H. Kulhari, S. K. Jain, R. Sistla and A. S. Chauhan, *Eur. J. Pharm. Sci.*, 2017, **96**, 84–92.
11 J. M. T. Van Griensven, R. C. Schoemaker, A. F. Cohen, H. G. Luus, M. Seibert-Grafe and H.-J. Röthig, *Eur. J. Clin. Pharmacol.*, 1995, **47**, 513–518.
12 S. Davis, in *xPharm: The comprehensive pharmacology reference*, ed. S. J. Enna and D. B. Bylund, Elsevier, New York, 2007, pp. 1–6.
13 Q. Pagneux, R. Ye, L. Chengnan, A. Barras, N. Hennuyer, B. Staels, D. Caina, J. I. Avila Osses, A. Abderrahmani, V. Plaisance, V. Pawlowski, R. Boukherroub, S. Melinte and S. Szunerits, *Nanoscale Horiz.*, 2020, **5**, 663–670.
14 F. Teodorescu, Y. Oz, G. Quéniat, A. Abderrahmani, C. Foulon, M. Lecoeur, R. Sanyal, A. Sanyal, R. Boukherroub and S. Szunerits, *J. Controlled Release*, 2017, **246**, 164–173.
15 F. Helal and M. E. Lane, *Eur. J. Pharm. Biopharm.*, 2014, **88**, 1–7.
16 Y. Ramesh and V. Sireesha, *J. Drug Delivery Ther.*, 2017, **7**, 56–65.
17 M. Zaman, U. Khalid, N. Ul Hassan Khan, K. Sultana, M. Hanif and K. Aftab, *EC Pharmacol. Toxicol.*, 2017, **4**, 20–32.
18 B. Zheng, Q.-Q. Fang, X.-F. Wang, B.-H. Shi, W.-Y. Zhao, C.-Y. Chen, M.-X. Zhang, L.-Y. Zhang, Y.-Y. Hu, P. Shi, L. Ma and W.-Q. Tan, *Biomed. Pharmacother.*, 2019, **118**, 109394.
19 K. Kitamura, M. Aihara, J. Osawa, S. Naito and Z. Ikezawa, *J. Dermatol.*, 1990, **17**, 44–51.
20 S. Shafiq, F. Shakeel, S. Talegaonkar, F. J. Ahmad, R. K. Khar and M. Ali, *Eur. J. Pharm. Biopharm.*, 2007, **66**, 227–243.
21 V. Préat and R. Vanbever, in *Transdermal Drug Delivery*, ed. R. H. Guy and J. Hadgraft, Marcel Dekker Inc., New York, 2003.
22 K. F. Alhasani, M. Kazi, M. A. Ibrahim, A. A. Shahba and F. K. Alanazi, *Int. J. Nanomed.*, 2019, **14**, 5435–5448.
23 S. Szunerits and R. Boukherroub, *Front. Bioeng. Biotechnol.*, 2018, **6**, 15.
24 L. Chengnan, Q. Pagneux, A. Voronova, A. Barras, A. Abderrahmani, V. Plaisance, V. Pawlowski, N. Hennuyer, B. Staels, L. Rosselle, N. Skandrani, M. Li, R. Boukherroub and S. Szunerits, *Nanoscale*, 2019, **11**, 15810–15820.
25 B. Demir, L. Rosselle, A. Voronova, Q. Pagneux, A. Quenon, V. Gmyr, D. Jary, N. Hennuyer, B. Staels, T. Hubert, A. Abderrahmani, V. Plaisance, V. Pawlowski, R. Boukherroub, S. Vignoud and S. Szunerits, *Nanoscale Horiz.*, 2022, **7**, 174–184.
26 F. Teodorescu, G. Queniat, C. Foulon, M. Lecoeur, A. Barras, S. Boulahneche, M. S. Medjram, T. Hubert, A. Abderrahmani, R. Boukherroub and S. Szunerits, *J. Controlled Release*, 2017, **245**, 137–146.
27 J. W. Lee, P. Gadiraju, J.-H. Park, M. G. Allen and M. R. Prausnitz, *J. Controlled Release*, 2011, **154**, 58–68.
28 B. P. Timko and D. S. Kohane, *Expert Opin. Drug Delivery*, 2014, **11**, 1681–1685.
29 P.-C. Wu, Y.-B. Huang, H.-H. Lin and Y.-H. Tsai, *Int. J. Pharm.*, 1996, **143**, 119–123.
30 J. B. O'Sullivan and S. B. Harrap, *Hypertension*, 1995, **25**, 162–165.

